Magnetic properties of free cobalt and gadolinium clusters

D. C. Douglass, A. J. Cox, J. P. Bucher,* and L. A. Bloomfield

Department of Physics, University of Virginia, Charlottesville, Virginia 22901

(Received 17 August 1992; revised manuscript received 6 January 1993)

We report the results of Stern-Gerlach-type magnetic deflection experiments on clusters of cobalt and gadolinium. Cobalt clusters exhibit superparamagnetic behavior over a broad range of temperatures, applied magnetic fields, and cluster sizes. We find an internal magnetic moment per atom of $2.24\pm0.14\mu_B$/atom for cobalt clusters containing 65–215 atoms at vibrational temperatures between 85 and 300 K, a value substantially in excess of the bulk value for cobalt. Over a similar temperature range, some gadolinium clusters exhibit superparamagnetic behavior while others exhibit behavior consistent with their moments being locked to their cluster lattices. In both cases, the internal magnetic moments per atom of gadolinium clusters are considerably reduced from the bulk value for gadolinium. The magnetic behaviors of many gadolinium clusters change qualitatively as their vibrational temperatures increase. We also address the current controversy concerning experimental cluster vibrational temperatures.

I. INTRODUCTION

There has been some controversy recently concerning the magnetic behavior of free ferromagnetic clusters.[1-3] While it is now generally agreed that ferromagnetic transition-metal clusters deflect toward a strong magnetic field following passage through a magnetic-field gradient, disagreement remains in understanding the origins of this behavior.

It is our view that the one-sided magnetic deflection of transition-metal clusters reflects the existence of thermal-relaxation processes within individual clusters. The central role of the vibrational temperature in establishing cluster magnetic behavior has been described previously,[3,4] along with a more recent report of temperature-dependent magnetic behavior in ferromagnetic rare-earth clusters.[5] In these papers it is proposed that the magnetic order present in transition-metal and rare-earth clusters manifests itself primarily in two types of finite-temperature particles: superparamagnetic clusters and clusters with their magnetic moments locked to the easy axes of their lattices.

Superparamagnetism occurs in small magnetically ordered particles when there is essentially no preferred direction for the overall magnetic moment of the system. While crystal anisotropy effects of the lattice always produce some anisotropy, the energies associated with the cluster lattice–magnetic-moment interaction are very small in transition-metal clusters. In all of the studies we have performed, clusters of cobalt, nickel, and iron have exhibited superparamagnetic behavior. Superparamagnetism is characterized by rapid orientational fluctuations of a particle's overall magnetic moment. Measurements that are performed on time scales long compared to the fluctuation time observe a time-averaged magnetic moment that responds paramagnetically to any applied magnetic field. Since it is the overall magnetic moment of the particle that responds, this behavior is called superparamagnetism.

If the temperature of a particle is reduced until the particle lattice–magnetic-moment interaction is large compared to the available thermal energy, superparamagnetism will no longer properly describe the particle's behavior. Below a certain temperature, the magnetic moment will not be able to fluctuate freely in orientation and will be constrained around a particular easy axis of the particle's lattice. At extremely low temperatures, the magnetic moment will become rigidly locked to that axis and will not fluctuate at all. We refer to this idea of rigid alignment between the cluster lattice and the magnetic moment as the locked-moment model. While locked-moment behavior has not yet been seen in transition metals, many rare-earth clusters do exhibit locked-moment behavior. Whether a rare-earth cluster appears superparamagnetic, locked-moment, or something in between depends critically on the cluster's size and vibrational temperature.

In this paper we describe studies of magnetic behavior in cobalt and gadolinium clusters. These studies are both more precise than the previous work and more extensive. The results of these studies confirm our previous observations of superparamagnetic and locked-moment behavior[3,5] and give evidence for increasingly subtle magnetic effects not adequately described by these simple models. Much of this work is based on a particular method for determining experimental cluster vibrational temperature, another matter of considerable recent controversy. In this paper, we also address this controversy by presenting the results of studies of rare-gas atom adsorption to metal clusters.

II. EXPERIMENT

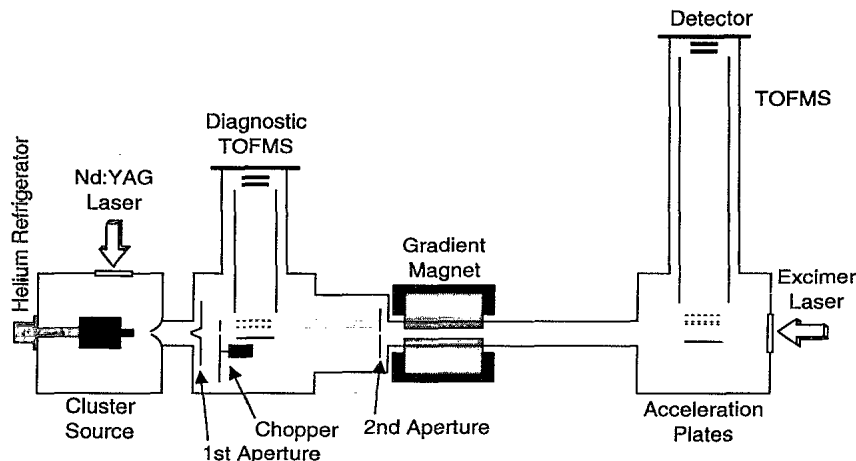The overall goal of the experiment is to observe the deflection of a cluster beam by a magnetic-field gradi-

FIG. 1. Experimental apparatus. Clusters are grown in the left vacuum chamber, collimated and chopped in the middle chamber, sent through the gradient magnet, and detected in the right chamber. The full length of the machine is approximately 3 m.

ent and to characterize this deflection as a function of such physical parameters as cluster size, chemical composition, temperatures, and applied magnetic fields. The apparatus used in this experiment appears in Fig. 1 and consists of four main sections: three high vacuum chambers and a magnet assembly. The metal cluster beam is formed in the first chamber, collimated and chopped in the second chamber, sent through the gradient magnet, and then analyzed in the third chamber. These four modules are described separately in the following four sections.

A. Cluster source

The cluster beam is formed in the first vacuum chamber by a laser vaporization cluster source (LVCS). Because cluster magnetic behavior is extremely sensitive to temperature, the source used in this experiment is designed to generate a beam of clusters with a well-defined vibrational temperature. Conventional LVCS designs grow clusters rapidly from a hot, laser-produced vapor and immediately turn these clusters into a molec-

ular beam. Growth is encouraged by the presence of helium gas, which cools the vapor and carries the resulting clusters out of the source in a free-jet expansion. If the growth and expansion occur too quickly, there is no time for the clusters to eliminate internal vibrational energy and the clusters leave the source vibrationally hot.[6] The free-jet expansion has at most only a modest effect on the cluster vibrational temperatures because there are far too few collisions between helium atoms and clusters during the expansion to maintain thermal equilibrium.[7]

Our source (Fig. 2) permits clusters to grow more slowly and to equilibrate thermally with their environment before undergoing a free-jet expansion into the surrounding vacuum chamber. This source has been described previously[8] and will be discussed here only in summary. Following vaporization of a portion of a metal sample disk by a Nd:YAG (yttrium aluminum garnet) laser pulse, clusters begin to grow in a helium-filled 0.5-cm^3 growth chamber. Helium is introduced into the chamber just before the laser pulse by a pulsed gas valve. The cluster-helium gas mixture slowly exits this chamber through a conical nozzle to form a supersonic beam. The beam lasts for several milliseconds, decaying in intensity
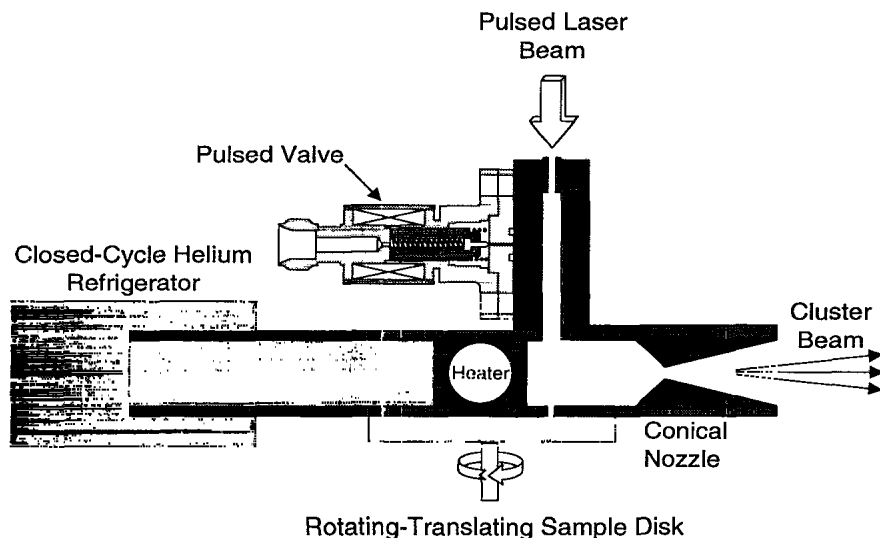

FIG. 2. The laser vaporization cluster source. Clusters are grown from a laser-produced vapor in the internal cavity above the sample disk. A pulse of helium gas is introduced into this cavity just before the laser pulse. The helium and cluster mixture can thermalize with the source before leaving the cavity through the conical nozzle.

roughly exponentially as the density of gas in the small chamber diminishes.

While clusters are present in the beam over a considerable fraction of this period, only the clusters that leave the source late in the cycle are in thermal equilibrium with the source itself. They have stopped growing long before they actually leave the source and have had sufficient time to cool vibrationally to the temperature of the surrounding helium gas. We refer to the time spent in the source, between the vaporizing laser pulse and the moment the clusters leave the nozzle as the residence time, τ_{res}. While the cluster beam intensity is significantly reduced at large τ_{res}, along with the gas density in the growth chamber, the benefit to us of knowing each cluster's vibrational temperature outweighs the disadvantage of reduced signal.

To obtain clusters with a particular vibrational temperature we adjust the temperature of the entire source, including the pulsed gas valve and its helium gas reservoir. The source is attached to a closed-cycle helium refrigerator (Cryomech AL10) and its temperature is regulated by an electronic temperature controller (Omega CN2001-A). A heating cartridge located in the source provides the heat input necessary to achieve regulation. The source itself is constructed out of 316 stainless steel, but it is encased in OFHC copper to reduce thermal gradients. With the refrigerator and temperature controller suitably adjusted, the temperature of the source can be regulated to within 2 K of any desired temperature between 58 K and 300 K. Reaching the lower temperatures requires shielding the source from room-temperature radiation. This shielding is achieved by enclosing the source in a liquid-nitrogen cooled copper box. The box serves not only to reduce radiative heating of the source, but also to cryopump contaminants such as water and to reduce the fraction of clusters that contain oxygen atoms.

B. Collimation and chopping

The cluster beam enters the second vacuum chamber through a 1.0-mm-diam molecular-beam skimmer. Inside this chamber, the cluster beam passes through two collimating slits, 0.851 m apart, that define the shape of the cluster beam before it enters the magnet assembly. The first collimating slit consists of two angled razor blades, 0.4 mm apart, that sweep unwanted gas away from the narrow stripe of usable clusters. The second collimating slit is a flat plate with four razor edges and a rectangular aperture 0.4 mm wide by 2.5 mm high.

Between the two collimating slits is a mechanical chopper wheel, 20 cm in diameter, that rotates 100 times per second and normally blocks the cluster beam. As it rotates, a narrow slit in the wheel traverses the cluster beam's path and permits the beam to pass for a period of about 100 μs. Together, the collimating slits and chopper wheel define a cluster packet that is very narrow in all directions: 0.4 mm wide, 2.5 mm high, and a few centimeters long.

C. Gradient magnet

Following collimation and chopping, the cluster beam passes through a gradient field magnet. This magnet is 250 mm long and has pole faces machined to create a quadrant of a quadrupole field (Fig. 3). The quadrupole field has several advantages over the more conventional two-wire gradient field.[9] The quadrupole field has a nearly uniform magnetic-field gradient over a large fraction of the region between the pole faces. The actual value of the magnetic field, despite having a gradient, varies smoothly across the open region.

It is thus possible to send a cluster beam of finite dimensions through the magnet and have it experience a nearly uniform magnetic-field gradient and a nearly constant magnetic field. A uniform gradient ensures that identical magnetic particles will undergo identical deflections, independent of their paths through the magnet. A nearly constant magnetic field ensures that any field-induced magnetic moments in the clusters will be similar for clusters passing through different regions of the space between the pole faces. While it is impossible to create a magnet that provides both a perfectly uniform gradient and a perfectly uniform applied field simultaneously, it would be difficult to improve on the compromise offered by the quadrupole field.

The magnet is constructed entirely out of chemically pure iron, having a carbon content of less than 0.01% (Inland Steel). With 23 031 At/m excitation, the magnet produces a peak magnetic field of 1.578 T and a gradient of 310.1 T/m. In the central region of the magnet, where the cluster beam is directed, the maximum magnetic field is 1.034 T. The magnetic field and field gradient were calibrated both with a Hall-probe magnetometer and by studying the deflections of several different magnetic atoms.

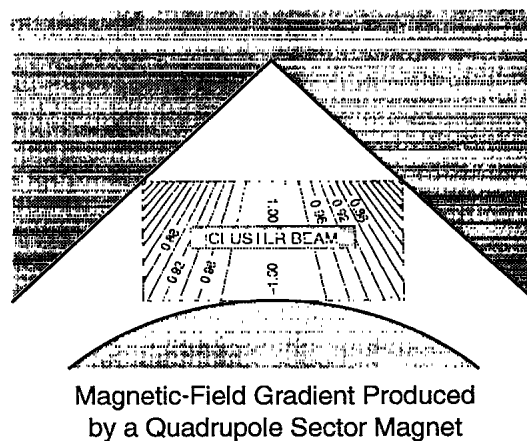Magnetic-Field Gradient Produced
by a Quadrupole Sector Magnet

FIG. 3. The gradient magnet used in these experiments. The shaded areas are the iron pole faces, which create a quadrant-of-a-quadrupole field (Ref. 9). The cluster beam travels through a central region of the gap, where the magnetic field and field gradient are particularly uniform. The labeled contours are lines of constant magnetic-field gradient.

D. Position measurement and mass analysis

The cluster beam then enters the ionization region of the time-of-flight mass spectrometer (TOFMS), located 1.183 m downstream from the gradient magnet. During their flight from magnet to mass spectrometer, clusters that experienced a transverse force in the gradient magnet will deflect away from their zero-field trajectories. To detect this deflection and to identify the clusters that deflect, the mass spectrometer is position sensitive. We collimated the beam of a 193-nm ArF excimer laser to a narrow stripe (0.5 mm wide) and scanned it across the cluster beam's transverse profile. Only those clusters that are exposed to the narrow laser beam are ionized, accelerated, and subsequently detected in the mass spectrometer. We record the mass spectra obtained as functions of the ionizing laser beam position to determine the spatial locations of each cluster size in the beam.

Only those clusters that are inside the ionization region of the mass spectrometer when the laser pulse arrives are detected. Because these clusters must have passed through the chopper when it was open, their flight time is well known. From this flight time, we can calculate their velocities and also deduce exactly when they left the source. We can thus determine their residence time in the source.

To determine the time-averaged projection of a cluster's magnetic dipole moment on the magnetic-field gradient, we measure that cluster's mass, m_{cluster}, velocity, v, and total deflection, d, as well as the magnetic-field gradient, dB/dz, the length of the magnet, L, and the length of the flight tube between the magnet and the mass spectrometer, D. We normally report the experimental magnetic moment *per atom*, μ_{expt}, obtained from

$$\mu_{\text{expt}} = \frac{dmv^2}{(dB/dz)(DL + L^2/2)}, \qquad (1)$$

where m is the mass of a single atom in the cluster. Working always with moments per atom makes it easier to compare the magnetic behaviors of clusters of different sizes and to relate their behavior with that of the bulk.

III. COBALT

When cobalt clusters pass through the gradient magnet, they all deflect to strong field by an amount that depends only on cluster size, vibrational temperature, and the applied magnetic field. Because clusters that share a common size and vibrational temperature deflect by the same amount, the effect of the gradient magnet is simply to shift the spatial profile of each cluster size toward the direction of strong magnetic field (Fig. 4). By the time clusters of a particular size arrive at the ionization region of the TOFMS, they have spread to form a packet with a spatial width of about 1.5 mm. The gradient magnetic field shifts this packet toward strong magnetic field. The shift is size dependent, with larger clusters shifting more than smaller clusters. However, clusters of a particular size all deflect by the same amount, indicating that their
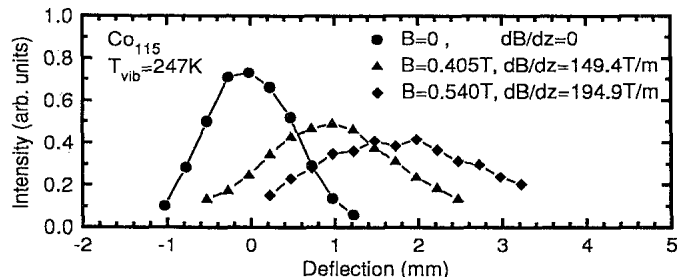

FIG. 4. Typical deflection profiles of cobalt clusters. Profiles are averages for $\text{Co}_{111-119}$, to reduce statistical noise, and were taken for several magnetic fields at $T_{\text{vib}} = 247$ K.

deflection does not depend on any detailed initial characteristics of the cluster, such as orientation or magnetic sublevel.

This homogeneous deflection of clusters sharing a common size and vibrational temperature is a consequence of their superparamagnetic behavior and will be explained in the theoretical part of this section. Before proceeding with this explanation, we will look at how the deflection depends on the three active parameters: cluster vibrational temperature, cluster size, and the applied magnetic field.

A. Experimental results

1. Temperature dependence

The hardest experimental parameter to control and measure is cluster vibrational temperature. Temperature has also been the most controversial aspect of these experiments. Prior to work on the magnetic structure of clusters, there were few ways known to measure cluster vibrational temperature directly.[10] Even in the case of magnetic measurements, our knowledge of vibrational temperature depends on a self-consistent match between experimental results and the superparamagnetic theory. If the superparamagnetic theory were wrong, then our claim to know the vibrational temperature of clusters would be without firm basis.

Fortunately, the superparamagnetic theory appears to be the correct explanation of magnetic behavior in clusters of the transition metals, so that our technique of temperature measurement is valid. Furthermore, our method of establishing a well-defined cluster vibrational temperature is similar to one proven to work recently by Hackett, who studied photoinduced thermionic emission in small clusters of refractory metals.[6] In what follows, we will assume that the superparamagnetic theory is correct and then show that the experimental and theoretical observations are self-consistent. At this point, it is only important to know that the superparamagnetic theory predicts an experimental cluster magnetic moment that is inversely proportional to its temperature, over a wide range of experimental conditions.

When we observe clusters of a particular size, at a set

value for the applied magnetic field, we find that their experimental magnetic moments increase with increasing residence time in the source. At very short residence times, we see almost no deflection of the clusters. The longer a cluster remains in the source, the more magnetic it appears. However, its magnetic moment does not increase without limit. Eventually the magnetic moment reaches a maximum value (Fig. 5). Increasing the residence time or varying other parameters of the source does not increase the magnetic moment beyond this value. The carrier gas pressure in the source growth chamber is still 30% to 60% of its peak value when the residence time associated with this magnetic saturation is reached,[8] eliminating pressure loss as the cause of the magnetic saturation.

We attribute this rise in magnetic moment with increasing time in the source to a decrease in cluster vibrational temperature. A cluster that leaves the source shortly after the vaporizing laser pulse is vibrationally hot and thus relatively nonmagnetic. After remaining in the source for approximately a millisecond, the cluster comes into thermal equilibrium with the source. This arrival at thermal equilibrium is signaled by the saturation of the cluster's magnetic moment. Further increases in residence time or changes in the free-jet expansion conditions do not affect the magnetic moment because they do not affect the cluster's vibrational temperature. Thus, like Hackett,[6] we find that the supersonic expansion has a negligible effect on the cluster vibrational temperatures.

To corroborate our notions of temperature, we performed rare-gas adsorption experiments similar to those of Milani and de Heer.[11] In their work, Milani and de Heer added argon gas to the helium carrier gas normally used in their source. With their source at room temperature, they observed one or more argon atoms adsorbed to many of the iron clusters arriving at their detector. The adsorption was particularly pronounced in clusters that left their source shortly after the vaporizing laser, when the gas pressure in the source was highest and the free-jet expansion most supersonic. They attribute this enhanced argon adsorption to a lower internal temperature for the clusters leaving their source at short residence times.

In our experiments, we also added a second rare gas to the helium carrier gas and looked for atoms of that second rare gas adsorbed to the clusters that reached our detector. In contrast to the work of Milani and de Heer, we

did not observe any argon adsorption to cobalt clusters, from Co_8 to Co_{150}.[12] We performed these experiments over a range of source temperatures from 73 K to 353 K and varied the percentage of argon atoms mixed into the helium carrier gas between 0.1% and 10%, as measured in the source chamber by a residual gas analyzer (Amatek, DYCOR model MA100 quadrupole gas analyzer). We took data at a variety of residence times for each temperature and argon percentage. We repeated these measurements using xenon as the second rare gas, but still saw no adsorption of xenon atoms to the clusters, regardless of source temperature, xenon atom percentage in the carrier gas, or cluster residence time in the source.

Because we cool the entire source, including the carrier gas reservoir, the argon or xenon has every opportunity to liquify or adsorb to the source itself before the supersonic expansion occurs. At the lowest temperatures, the vapor pressure of argon or xenon limits the percentage of that gas that we can mix with helium. If we increase the argon or xenon percentage, we liquify that gas in the source and the source clogs up.

These rare-gas adsorption experiments indicate that the clusters leaving our source are unable to compete favorably for adsorption of the rare-gas atoms. We must avoid temperature/pressure regimes in which the rare gas adsorbs to or liquifies in the source. When we do, we do not detect any cobalt clusters that have adsorbed rare-gas atoms. While we know from the residual gas analyzer that rare-gas atoms are leaving the source, we also know that they are not adsorbed to the cobalt clusters by the time those clusters reach the mass spectrometer. If we increase the rare-gas percentage or reduce the source temperature, the source plugs up. Evidently, we cannot enter the regime of low temperature or large rare-gas percentage needed to observe rare-gas atom adsorption. Before the rare-gas atoms will stick to the clusters, they stick to the source or to themselves and plug the source.

From this result, we deduce that the vibrational temperatures of our clusters are never significantly less than the temperature of our source, regardless of residence time. If they were, we should detect rare-gas atoms adsorbed to some of the clusters. This lower limit on cluster vibrational temperature, which is the temperature of the source itself, is further evidence that the supersonic expansion in our source has essentially no effect on the vibrational temperatures of our clusters.

To explain this apparent discrepancy between our observations and those of Milani and de Heer, we should note that their source is somewhat different from ours and that the free-jet expansion that occurs in their source may be much more supersonic than that in our source. While this enhanced supersonic expansion might lead to dramatically better cooling of the metal clusters themselves, there is a second possible explanation for their observations.

If the free-jet expansion in their source is strong enough and the atom fraction of argon in the carrier gas is high enough, argon itself will cluster during the expansion. Collisions will then occur between very cold argon clusters and hot metal clusters, to produce mixed systems. A
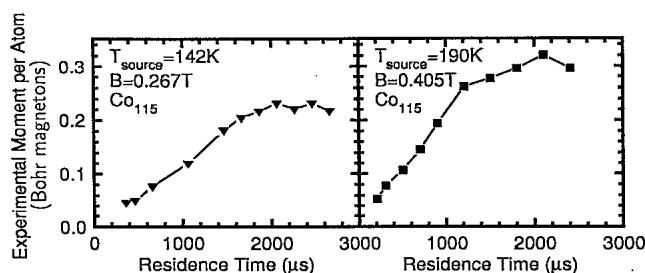

FIG. 5. Experimental magnetic moment per atom as a function of τ_{res} for two different source temperatures.

mixed system of this sort will be unstable against evaporation. During the next few milliseconds, most of the argon atoms will boil away, leaving behind a very cold metal cluster with a few remaining argon atoms. These evaporated mixed clusters may be what Milani and de Heer observe at their detector.

Mixed clusters produced by the evaporation mechanism will be quite cold, since most of their vibrational energies will have been removed by the evaporation process. However, their presence in the cluster beam only indicates that the free-jet expansion is supersonic enough to initiate argon clustering. Shortly after the carrier gas has been introduced into the source, the free-jet expansion will be most intense and the density of argon clusters it produces will be highest. Milani and de Heer observe more rare-gas atom adsorption to their metal clusters at such short residence times. Thus, while we cannot rule out genuine cooling of pure metal clusters by the supersonic expansion in their source, this alternative mechanism for adsorbing argon atoms to metal clusters is entirely consistent with their experimental results. Although the evaporation mechanism is interesting and would produce very cold clusters, final temperatures of the metal clusters would not be known accurately and would bear little resemblance to their temperatures before they collided with the argon clusters.

Based on our studies of cluster magnetic moments versus residence times and on the rare-gas adsorption experiments, we feel entirely justified in assuming that clusters leaving our source at very long residence times are in thermal equilibrium with the source. Unfortunately, by the time the clusters have reached thermal equilibrium with the source, their density has diminished and the cluster signal is reduced. However, recent improvements in our cluster source have made it possible to perform detailed measurements at long residence times. Unlike our previous work,[3] all of the measurements presented in this paper were performed with τ_{res} long enough to ensure that the clusters were in thermal equilibrium with the source. We verified that we had obtained thermal equilibrium at each source temperature and mass range by studying experimental magnetic moments as functions of residence time and always waiting until the magnetic moments had reached their maximum values. Examples of such residence time studies appear in Fig. 5. It should be noted that the observed moment continues to decrease as the residence time decreases. In no case was an anomalous increase of the moment observed, even at the shortest residence times obtainable.

Because we can establish the vibrational temperature of the clusters with reasonable confidence, we can study the change in μ_{expt} as a function of temperature T. Figure 6 shows μ_{expt} as functions of T and $1/T$. The observed moment increases linearly with $1/T$. This dependence is precisely the prediction of the superparamagnetic theory.

However, we must note that we were unable to make meaningful measurements below about 85 K. Although there appears to be an abrupt increase in magnetic moment as the source temperature drops below 85 K, that magnetic moment becomes dependent on the expansion
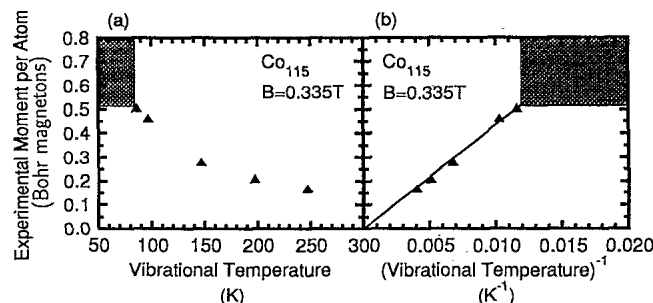

FIG. 6. Experimental magnetic moment per atom versus (a) temperature and (b) inverse temperature. The data were taken with an applied magnetic field of 0.335 T and a field gradient of 126.6 T/m. The shaded area for temperatures below 85 K indicates that, while large magnetic moments per atom are observed below this temperature, they are dependent on source conditions and do not saturate at long residence times (see text).

conditions. The magnetic moment continues to increase with increasing τ_{res} and no longer saturates. Increasing the helium gas pressure in the source affects the measured magnetic moment at a given source temperature and also increases the source temperature at which this anomalous behavior first appears. The peak profiles are indistinguishable in form from data taken at higher source temperatures and similar peak-center deflections. No transition to a different magnetic behavior is observable in the peak profiles.

Such peculiar behavior could be due to one of three things. First, in a superparamagnetic particle, the experimental magnetic moment per atom depends on the internal magnetic moment per atom. While we expect this internal moment per atom to be constant throughout the range of temperatures we study, a sudden rise in the internal moment per atom at low temperatures would produce the observed effect.

Second, the magnetic moment could be starting to couple to the cluster lattice, so that the superparamagnetic model is no longer applicable. This coupling process is seen in many rare-earth clusters and will be discussed in the sections on gadolinium clusters.

Third, there could be some secondary cooling mechanism active so that the clusters are somewhat colder than the source temperature. The most likely secondary cooling mechanism would be the attachment of helium atoms or helium clusters to the surface of the cobalt clusters during the supersonic expansion. These adsorbed helium atoms would evaporate in flight, taking energy away from the remaining cobalt cluster.

Given our inability to adsorb argon or xenon to cold clusters, the third case seems unlikely. It is our view that the second explanation is the most probable. Even if the magnetic moment were beginning to lock to the cluster lattice, the peak shape would not change noticeably because the moment would be only partially coupled to the cluster lattice at these temperatures. Only at much lower temperatures would the full locked-moment deflection profile appear. There also is no way to completely

rule out the first behavior except by taking data at even lower temperatures. Unfortunately, we are currently unable to reduce the cluster source temperature below 58 K.

2. Size dependence

Figure 7 shows μ_{expt} as a function of cluster size N for clusters ranging from Co_{33} to Co_{215}. Again, the curve is very linear. The magnetic field and gradient were chosen so that the largest clusters were deflected as far as could be measured reliably. At the same experimental conditions, the smallest clusters did not deflect very much. Because of the difficulties involved in measuring μ_{expt} for clusters that do not deflect very far, the data in Fig. 7 have relatively large uncertainties at the small cluster end and the curve appears noisy in that region.

Figure 8 shows the smaller clusters at several different fields. The smaller clusters show some interesting behavior. The observed magnetic moment per atom as a function of N has a step around Co_{55}. This step is most evident in the top data set in Fig. 8, and while it is small, it is very reproducible. Several packing schemes, including fcc and icosahedral structures, form highly symmetrical, closed shell structures in the vicinity of the 55-atom cluster. The step in the magnetic properties near Co_{55} could indicate an evolution with increasing size from one underlying cluster symmetry to another. An abrupt dip in the number of NH_3 molecules that will bind to cobalt clusters has also been observed in this same size range.[13]

In previous work,[3] we stated that we had resolved two magnetic deflection peaks for clusters ranging from Co_{55} to Co_{66}. We attributed these two peaks to the presence to two isomers in the cluster beam. We have been unable to reproduce these doublets, perhaps due to subtle changes in the growth conditions that occurred when we redesigned the source for use in the present work. The previous data were not taken using long τ_{res}, which may also have something to do with the disappearance of the magnetic doublets. As noted above, though, the abrupt rise at $N = 56$ continues to be reproducible.
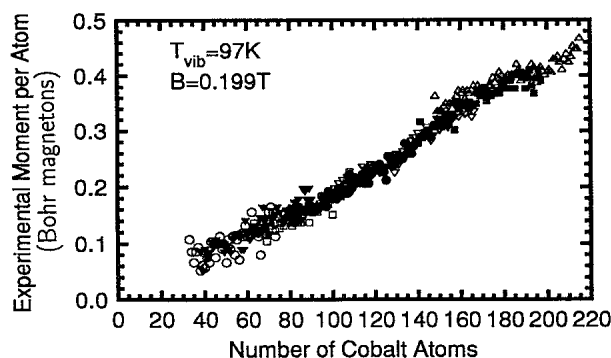
FIG. 7. Experimental magnetic moment per atom versus cluster size, for $33 \leq N \leq 215$. The applied field is 0.199 T, and the gradient is 78.5 T/m. The data were taken with $T_{vib} = 97$ K.
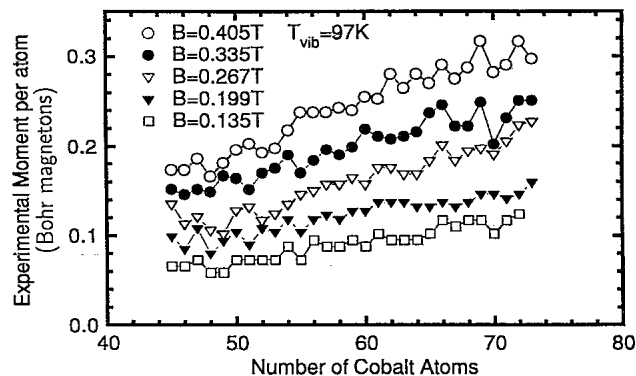
FIG. 8. Experimental magnetic moment per atom versus cluster size, taken at several different applied fields. Note the step around N=55. The data were taken with $T_{vib} = 97$ K.

3. Applied field dependence

Figure 9 shows the dependence of μ_{expt} on applied magnetic field. Results are presented over a wide range of cluster sizes at 97 K, and at two different temperatures for $N = 115$. In all cases, μ_{expt} increases linearly with increasing field. As discussed above, the observed magnetic moments per atom are larger at the lower temperatures and in the larger clusters.

B. Theory of superparamagnetism

These results are quite different from what was initially expected theoretically. Small ferromagnetic clusters were expected to have permanent magnetic moments per atom that were larger than the bulk value. In cobalt, this bulk value is $1.71\mu_B$/atom. The magnetic moments per atom were also expected to be relatively insensitive to cluster size or any applied magnetic field. It was thus something of a surprise when iron[2] and cobalt[3] clusters were found to have magnetic moments per atom that depended strongly on cluster size, applied magnetic field, and cluster temperature, and were considerably less than the bulk values.

Fortunately, the theoretical predictions and the experimental results are nicely reconciled by the concept of superparamagnetism. Superparamagnetism has been
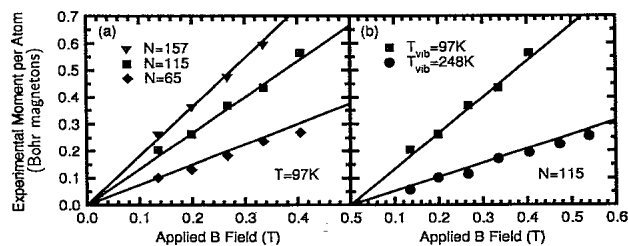
FIG. 9. Experimental magnetic moment per atom versus magnetic field. (a) $T_{vib} = 97$ K for $N = 65$, 115, and 157. (b) $N = 115$ for $T_{vib} = 97$ K and 247 K.

observed and understood in supported particles for several decades[14] but was first proposed for free clusters by Khanna and Linderoth in 1991.[4] A superparamagnetic cluster's internal magnetic moment may be quite large, but that moment's orientation is not fixed to the cluster lattice. In the presence of thermal excitations, the magnetic moment fluctuates rapidly in orientation and explores the entire Boltzmann distribution of permitted orientations in a very short time. An experiment that measures the magnetic moment slowly in comparison to the fluctuation time scale observes the time-averaged magnetic moment, which is reduced from the internal magnetic moment by the Langevin function.

When a ferromagnetic particle is small enough ($\leq$ 10^5 atoms) and the ambient temperature is high enough ($\geq$ 50 K), the energy of interaction between the particle's magnetic moment and its lattice can become small compared to k_BT. Thermal excitations can then redirect the magnetic moment away from any easy axis of the particle. The particle's single "super" moment is able to orient in any direction relative to the cluster lattice, with all directions being nearly equal energetically. The moment fluctuates under thermal agitation, and since all directions are equally probable, there is no zero-field magnetic moment. Superparamagnets, like all paramagnets, are soft magnetic objects that retain no memory of previous magnetizations and have no area under their hysteresis curves.

The phenomenon of superparamagnetism found in ferromagnetic clusters is completely analogous to classical Langevin paramagnetism. A superparamagnetic particle simply has one magnetic moment for the entire particle. This moment is essentially free to point in any direction relative to the particle lattice. When a magnetic field is applied, the moment tends to align with the applied field. However, what really changes is the Boltzmann distribution of possible orientations. In the presence of an external field, the Boltzmann distribution is no longer isotropic and the time-averaged moment begins to point in the direction of the applied field. Only at extremely high fields or very low temperatures will the time-averaged magnetic moment approach the full internal magnetic moment of the cluster.

Consider a cluster with N atoms and a magnetic moment per atom of μ. The total magnetic moment of the cluster is then $N\mu$, and the total magnetic energy U in an applied field is $U = -N\mu \cdot \mathbf{B}$, where we neglect any small crystal anisotropy effects. For sufficiently large clusters (i.e., $N\mu \gg \mu_B$), the problem is essentially classical and μ and $\mathbf{B}$ can assume any relative orientation. Averaging over all angles, weighted by the Boltzmann factor, gives rise to the Langevin function. The average projection of the magnetic moment per atom μ_{eff} along the field axis is μ times the Langevin function,

$$\mu_{\text{eff}} = \mu\mathcal{L}\left(\frac{N\mu B}{kT}\right) = \mu\left[\coth\left(\frac{N\mu B}{kT}\right) - \frac{kT}{N\mu B}\right]. \quad (2)$$

For $N\mu B/kT \ll 1$, this equation is approximately

$$\mu_{\text{eff}} \approx \frac{N\mu^2 B}{3kT}. \quad (3)$$

Thus, while a superparamagnetic particle has an internal magnetic moment per atom μ, any experiment that measures the time-averaged projection of this moment on the magnetic-field axis will observe an effective magnetic moment per atom μ_{eff}.

C. Summary for cobalt

Figure 10 shows data taken from Figs. 6 and 9 plotted versus NB/T. This plot allows us to relate the measured magnetic moment per atom, μ_{expt}, to the effective magnetic moment per atom, μ_{eff}, defined by the superparamagnetic model. The straight line is a least-squares fit to the data, from which the internal magnetic moment per atom, μ, of the cobalt clusters can be calculated using the superparamagnetic model. We find the internal magnetic moment per cobalt atom to be $2.24 \pm 0.14\mu_B$/atom, independent of cluster size from Co_{56} to Co_{215}. The total uncertainty represents a 5% uncertainty in the experimental magnetic moment, a 6% uncertainty in the field calibration, a 2% uncertainty in the vibrational temperature, and a 2% field and gradient uncertainty due to possible misalignment of the gradient magnet. The only possible systematic error that we cannot entirely rule out is a mismeasurement of cluster vibrational temperature. If the cluster vibrational temperatures are always lower than what we believe, then we are overestimating the internal magnetic moment per atom. However, for us to be wrong in our analysis of temperature and yet have Fig. 6 show a very linear dependence of μ_{expt} on $1/T$, the actual vibrational temperatures of the clusters must always differ from the value we report by the same *percentage*, regardless of the source temperature. We believe that this possibility is very unlikely.

One interesting corollary to this agreement between the superparamagnetic model and the experimental results is that the internal structure and dynamics of the clusters do not significantly complicate their magnetic
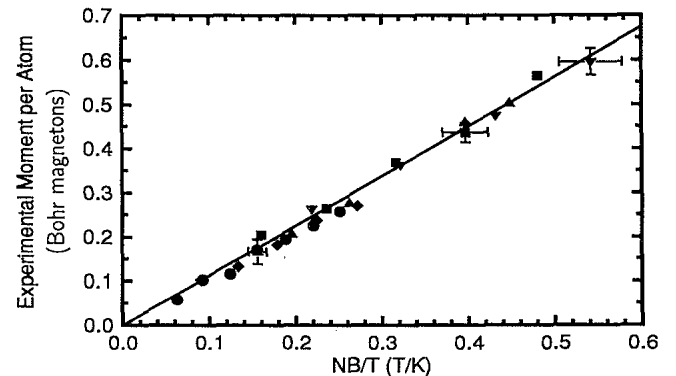

FIG. 10. Experimental magnetic moment per atom versus $\frac{NB}{T}$. The data points are those plotted in Figs. 6 and 9 and the line is a least-squares fit of the data points. Note that the data points fit the line very well, and that the line passes through the origin.

behaviors. The internal magnetic moment per atom of a cluster is well described by a single value, μ. For most purposes, the cluster behaves as though it has just one giant magnetic moment. We find that μ is essentially temperature independent for cobalt but slightly temperature dependent for gadolinium, as will be discussed below.

The results obtained by de Heer, Milani, and Chatelain[2] on iron clusters share many similarities with our results. They observe an increase in the observed moment with both cluster size and applied field. They also observe an increase in the observed moment which is related to the residence time, though they did not measure this parameter while taking the data. Unfortunately, they are unable to work at different source temperatures. They are able to cool their nozzle with liquid nitrogen, but it is unclear that this is sufficient to cause their clusters to reach thermal equilibrium at 77 K. Still, they claim that clusters early in the pulse are colder than clusters late in the pulse, as the "fast" clusters are cooled better by the supersonic expansion. We see no evidence that short residence time clusters are colder than long residence time clusters, either indirectly from magnetic-moment experiments or directly via argon or xenon attachment.

At large residence times, when their iron clusters should be in thermal equilibrium with their source, they observe a magnetic moment of about $0.8\mu_B$ for $N = 120 - 140$, $B = 1.1$ T, and $T_{\mathrm{vib}} = 300$ K. Using Eq. (3), we can determine that the true moment per iron atom is about $2.7\mu_B$ per atom. This value is in very good agreement with our own preliminary result of $2.92 \pm 0.28\mu_B$ per atom from $T = 100 - 300$ K.[15]

In our previous work, we reported a value of $2.08 \pm 0.20\mu_B$/atom for internal magnetic moment per cobalt atom.[3] A vast majority of the measurements used in that work were taken at residence times too short to reach thermal equilibrium and with a source that was prone to significant thermal gradients. As a result, the temperature uncertainties in our earlier work were much greater than the uncertainties in the present work.

IV. GADOLINIUM

The rare-earth solids exhibit a variety of magnetic behaviors that is far richer than that of the transition metals. Magnetism in the lanthanides is due almost entirely to $4f$ electrons, which tend to be localized at the rare-earth ions. These $4f$ electrons couple to those on nearby ions through the mechanism of indirect exchange, the RKKY interaction.[16,17] Because the RKKY interaction is mediated by the conduction electrons, it is very sensitive to the structure and filling of the conduction bands. Thus, small changes in the band structure of a solid can have dramatic effects on the magnetic properties of that solid.

Gadolinium has a magnetic moment per atom in the bulk of $7.55\mu_B$/atom. This large magnetic moment per atom is so nearly localized at individual ion sites that we can expect similar magnetic moments per atom in gadolinium clusters. What we should not expect is that

the RKKY interaction that couples the moments of adjacent ions should be unaffected by the reduced dimensions of the system. In clusters, the structure and filling of the conduction band will be different from that in the bulk metal and may give rise to very different magnetic ordering in the clusters.

It should come as no surprise that rare-earth clusters exhibit a rich variety of magnetic behaviors. Here we report studies of gadolinium clusters between Gd_{10} and Gd_{35}. This range was chosen largely for practical reasons. At the long residence times needed to reach thermal equilibrium, our cluster source produces relatively few clusters smaller than Gd_{10}. In order to study pure clusters, without any impurity atoms such as oxygen, the mass spectrometer must be able to resolve the pure metal cluster peak from the oxidized cluster peak. Unfortunately, the large number of naturally occurring gadolinium isotopes makes it difficult to distinguish pure clusters from oxidized clusters beyond about Gd_{35}.

A. Experimental results

As noted in the Introduction, we observe two distinct magnetic behaviors for gadolinium clusters. Some cluster sizes behave superparamagnetically while others have magnetic moments that are locked to their lattices. We also observe transitions between these two behaviors as we change the cluster vibrational temperatures.

The size specificity of the behavior is immediately evident in the mass spectra observed on and off the cluster beam axis when the gradient magnet is on. Such mass spectra appear in Fig. 11. With the gradient magnet turned off [Fig. 11(a)], there is essentially no structure to the mass spectrum. Except for a slightly elevated abundance of Gd_{13}, the mass spectrum shows only the overall detection envelope of the apparatus when optimized to observe clusters near Gd_{20}.

However, with the gradient magnet turned on, most of the gadolinium clusters disappear from the beam axis, leaving Gd_{22}, Gd_{30}, and Gd_{33} significantly more abundant than their neighbors [Fig. 11(b)]. Where did the missing clusters go? The missing gadolinium clusters are deflected toward both strong and weak magnetic field, in a manner that is not consistent with superparamagnetism. In Fig. 11(c), the mass spectrum taken far from the beam axis on the strong field side now contains some of the missing clusters. The three clusters that remained near the beam axis are nearly absent from this off-axis spectrum.

The small peaks in Fig. 11 at half-integer numbers of gadolinium atoms are doubly ionized gadolinium clusters appearing at half their mass in the mass spectra. This ambiguity of mass can cause trouble when we try to identify which clusters are where. If there are many Gd_{22} clusters present as we study Gd_{11}, we will be troubled by an inability to distinguish Gd_{22}^{++} from Gd_{11}^{+} in the mass spectrometer. Such an ambiguity is visible in Fig. 11(b), where Gd_{11} appears to be unusually abundant on the beam axis. In fact, this apparent increase is actually an increase in Gd_{22}^{++}, not Gd_{11}^{+}. Because rare-
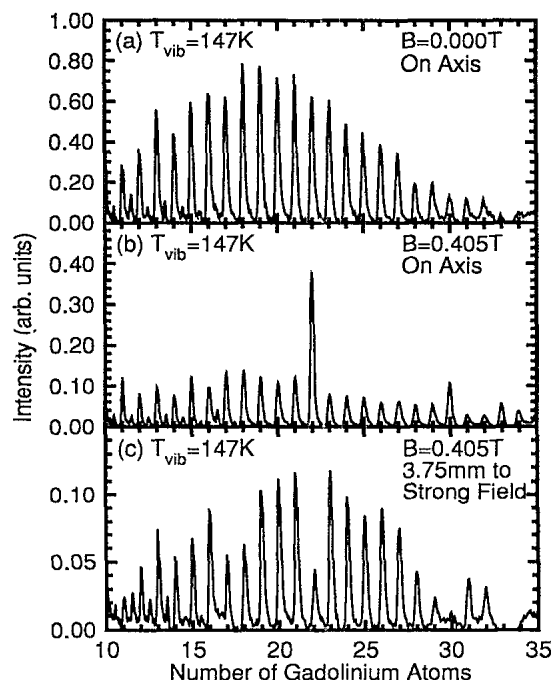
FIG. 11. Gadolinium mass spectra, taken with $T_{vib} = 147$ K (a) on the beam axis with no applied field, (b) on the beam axis with an applied field, and (c) at the same applied field as in (b), but shifted 3.75 mm toward the strong field side of the magnet.

FIG. 12. Deflection profiles for Gd_{22} and Gd_{23} at three different values of the applied magnetic field. The solid lines are fits to the Gd_{23} profiles, based on the locked-moment model. All three data sets were taken with $T_{source} = 147$ K.

earth clusters are easy to doubly ionize, we must always be careful to adjust the apparatus so that there are few clusters present at twice the mass of the clusters we are actively studying. We also use ionizing laser intensities low enough to avoid most double ionization.

The magnetic behavior of most gadolinium clusters is much more complicated than that of superparamagnetism. The cluster packets do not simply shift toward strong magnetic field. Instead, they spread out over a very broad range of deflections. To understand what is happening, complete beam deflection profiles are needed. We obtain these deflection profiles by measuring the intensity of each cluster size as a function of transverse distance from the zero-field beam position. Because rare-earth clusters deflect to both strong and weak field, we look for the clusters on both sides of the zero-field position.

Several profiles obtained in this manner are shown in Fig. 12. In this figure, profiles are shown for Gd_{22} and Gd_{23} for three different applied magnetic fields at $T_{vib} = 147$ K. The profiles for Gd_{23} are all very broad, and their shapes depend on the applied field. At low fields, a small fraction of the clusters deflects to the weak field side. These broad profiles are consistent with the predictions of a model in which the magnetic moment is locked to the cluster lattice and that moment rotates with the cluster. The theory of locked-moment clusters is described in some detail in Sec. IV B. The solid lines in Fig. 12 are fits to the Gd_{23} profiles obtained from this theory.

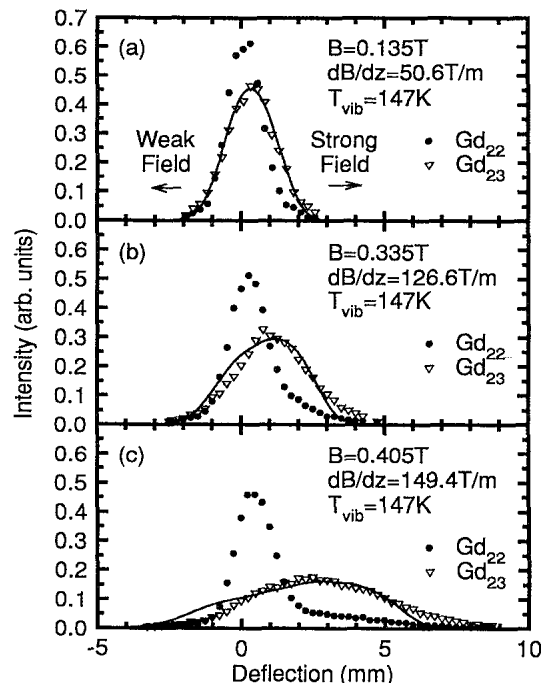## 1. Gd_{22}

The profiles of Gd_{22} have two components. The minor component exhibits the same broad deflections as Gd_{23}. The major component behaves quite differently: it is superparamagnetic. As with the superparamagnetism of cobalt clusters, the fraction of Gd_{22} clusters that contribute to this relatively sharp peak deflects uniformly to the strong field side. There is little broadening of the profile as a function of field and the center of the peak is a good measure of the deflection of the beam as a whole. We observe a saturation of the deflection as a function of τ_{res}. μ_{expt} increases with increasing τ_{res} until a maximum value is reached. Further increases in τ_{res} have no effect on μ_{expt}. Once again, we assume that the clusters have reached thermal equilibrium with the source at this value of τ_{res}. We use the saturation of μ_{expt} for the superparamagnetic Gd_{22} clusters as an indication that the clusters' vibrational temperatures have come into equilibrium with that of the source. All the data presented in this paper were obtained at sufficiently large τ_{res} to ensure that the clusters were in thermal equilibrium with the source. The cluster vibrational temperatures are assumed to be those of the source.

As expected for a superparamagnetic particle, the value of μ_{expt} for Gd_{22} increases linearly with applied magnetic field (Fig. 13). The deviations from linear behavior, although suggestive of some more complicated behavior, are probably simply noise. At very low magnetic fields and small deflections, the overlap of the superparamagnetic component and the other, non-
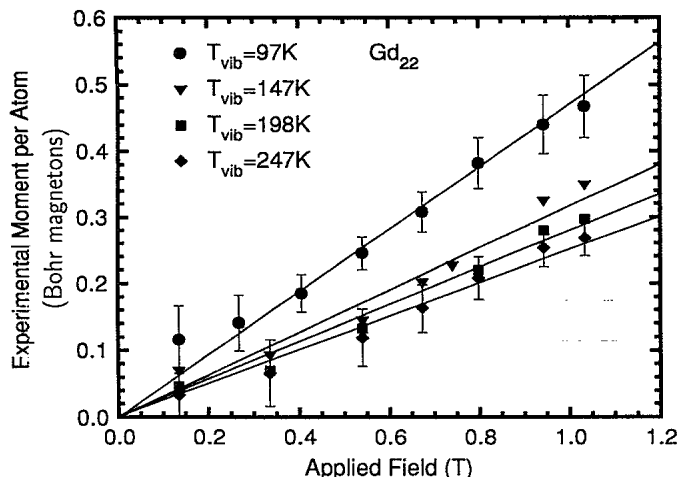
FIG. 13. Experimental magnetic moment per atom of the superparamagnetic component of Gd_{22} versus applied magnetic field, for several different vibrational temperatures. Error bars are given for only two data sets to avoid confusion. The straight lines are linear least-squares fits to the data.

superparamagnetic component makes it very difficult to obtain an accurate value for μ_{expt}.

However, when we vary the vibrational temperature while keeping the applied field constant, we see a clear deviation from the linear behavior predicted by superparamagnetism (Fig. 14). μ_{expt} is not proportional to $1/T$. This deviation is statistically significant and reproducible. It is the hallmark of something we have heretofore neglected: a temperature dependence of the cluster's internal magnetic moment per atom, μ. In the transition metals, we safely assumed that the internal magnetic moment per atom was temperature independent. In a ferromagnetic system, the internal magnetic moment per atom should remain almost constant near zero temperature but diminish as the Curie temperature is approached from below. The Curie temperature for bulk cobalt is 1404 K so that μ is probably extremely
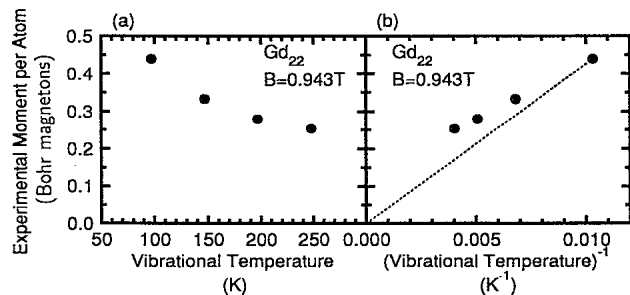

FIG. 14. Experimental magnetic moment per atom of the superparamagnetic component of Gd_{22} versus (a) vibrational temperature and (b) inverse vibrational temperature, for several different fields. The dashed line in (b) is the prediction of the superparamagnetic model if μ remains constant, independent of temperature.

close to its maximum, zero-temperature value at our experimental vibrational temperatures.

In bulk gadolinium, the Curie temperature is only 293 K. It seems very likely that μ should change substantially over the range of temperatures investigated. What is puzzling, however, is that the internal magnetic moment per atom of Gd_{22} increases with increasing temperature (Table I). If the magnetic order in Gd_{22} were pure ferromagnetism, we would expect increasing vibrational temperature to reduce the moment slowly toward zero.

The first complication in this simple picture is due to finite-size effects. In a finite-sized ferromagnetic system, the magnetic moment per atom does not reach zero at the Curie temperature.[18] Although the individual magnetic moments that form the overall ferromagnetic moment are essentially decoupled by thermal fluctuations, there are not enough of them to ensure statistical cancellation of their magnetic moments. As a result, the average magnetic moment of a finite ferromagnetic system remains somewhat more than zero. But the trend is always toward decreasing magnetic moment with increasing temperature.

In a finite antiferromagnetic system, the trend is reversed. At very low temperature, the individual magnetic moments nearly cancel one another and the average magnetic moment per atom is close to zero.[19,20] But as the temperature of the finite system increases, the decoupling of individual magnetic moments causes the average internal magnetic moment per atom to approach the same value as in the ferromagnetic case.[20] The internal magnetic moment per atom actually increases with increasing temperature.

If the internal magnetic moment per atom μ of a superparamagnetic particle increases with temperature, then the observed magnetic moment μ_{eff} will not decrease as $1/T$. μ_{eff} will be larger at high temperatures than it would be if μ were temperature independent. The agreement between the experimental behavior of gadolinium clusters and the predictions of model calculations suggests that the magnetic order in gadolinium clusters is at least partially antiferromagnetic.[20] An antiferromagnetic coupling in gadolinium clusters would also explain why the internal magnetic moments per atom that we observe are much less than the bulk value. Bulk gadolinium is not antiferromagnetic at any temperature.

2. Gd_{17}

The simultaneous presence of both superparamagnetic and locked-moment behaviors in a single cluster size in-

TABLE I. Internal magnetic moment per atom of the superparamagnetic component of Gd_{22}. The moment appears to continue to increase at 300 K, but the observed deflections are too small to be considered reliable.

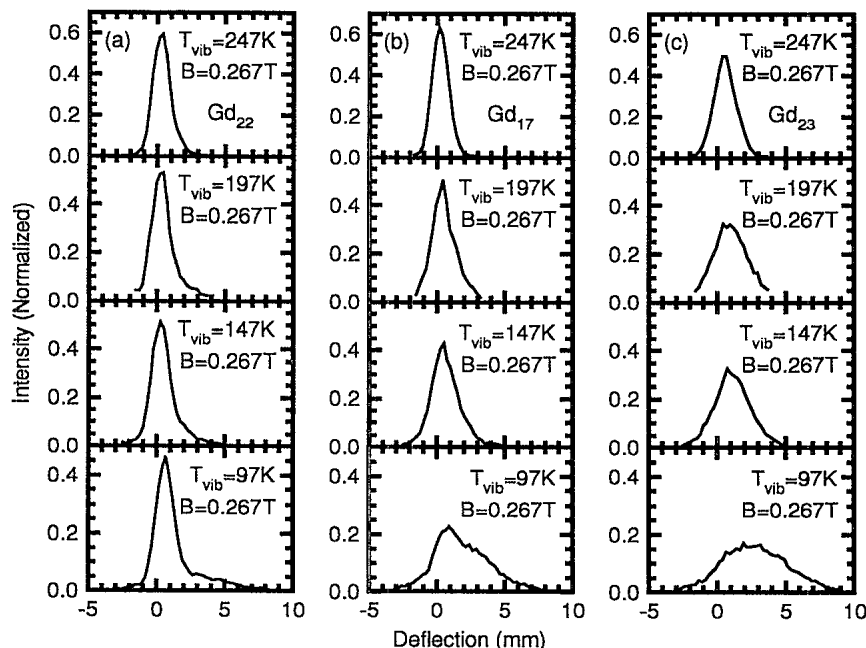| T_{vib}	μ
97 K	$2.94\pm0.35\mu_B$/atom
147 K	$3.33\pm0.40\mu_B$/atom
198 K	$3.65\pm0.44\mu_B$/atom
247 K	$3.88\pm0.47\mu_B$/atom

FIG. 15. Gd_{17}, Gd_{22}, and G_{23} profiles, for four different vibrational temperatures. The applied magnetic field is 0.267 T and the field gradient is 101.3 T/m. Gd_{17} undergoes a transition from locked-moment behavior at low temperature to superparamagnetic behavior at high temperature.

dicates that there are at least two distinguishable groups of clusters sharing the same number of atoms. These groups could correspond to two different isomers, either magnetic or structural, that are present in the beam. By magnetic isomer, we are referring to clusters that share similar spatial structures but have adopted somewhat different magnetic orderings or orientations.

Regardless of what mechanism distinguishes these groups of clusters, we find that the two behaviors merge together as the vibrational temperature increases. Clusters that exhibit locked-moment behavior at low temperature become superparamagnetic at high temperature. This type of transition is exemplified by Gd_{17}. At 97 K, Gd_{17} exhibits almost pure locked-moment behavior. At room temperature, Gd_{17} is nearly pure superparamagnet. We observe a gradual transition from locked-moment cluster to superparamagnet between 100 K and 200 K.

This transition is seen in Fig. 15, where we show deflection profiles of Gd_{17}, Gd_{22}, and Gd_{23} at four different temperatures. Gd_{22} is predominantly superparamagnetic at all temperatures and Gd_{23} is predominantly locked-moment at all temperatures. At the lowest temperature, 97 K, the profile of Gd_{17} resembles that of Gd_{23}. Both are predominantly locked-moment. At the highest tem-

perature, 247 K, the profile of Gd_{17} resembles that of Gd_{22}. Both are predominantly superparamagnetic. At the two intermediate temperatures, 147 K and 197 K, Gd_{17} exhibits a behavior that is intermediate between the two ideal behaviors.

We note that, in Fig. 15, the applied magnetic field was the same for all temperatures. Because the cluster beam moves much faster at 247 K than at 97 K, the deflections are much smaller at 247 K than they are at 97 K. As a result, the 247-K profiles are severely limited by the experimental transverse width of the zero-field cluster beam. To see the magnetic behaviors more clearly at high-temperature, we must increase the magnetic field. Figure 16 shows the high-temperature behavior quite clearly. At 303 K, Gd_{22} and Gd_{17} exhibit the relatively narrow profiles of clusters that are predominantly superparamagnetic while Gd_{23} continues to exhibit the broad profile of a locked-moment cluster.

3. Other clusters

Other clusters from Gd_{11} to Gd_{30} behave in much the same way as Gd_{17}, Gd_{22}, or Gd_{23}. They exhibit one or
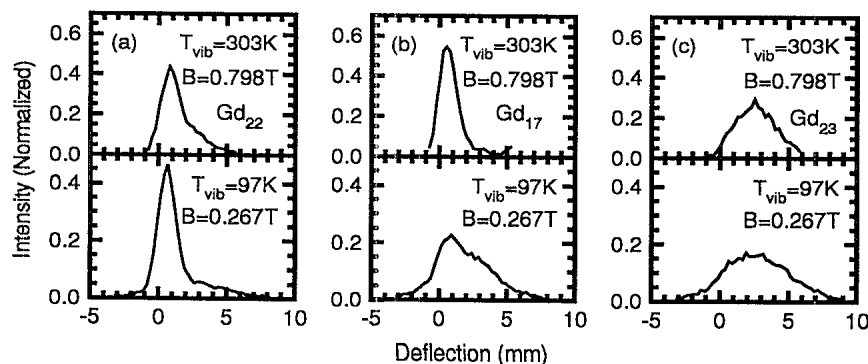

FIG. 16. Gd_{17}, Gd_{22}, and G_{23} profiles, for two different vibrational temperatures and applied fields. At 303 K, $B = 0.779$ T and $dB/dz = 263.3$ T/m. At 97 K, $B = 0.267$ T and $dB/dz = 101.3$ T/m. The transition of Gd_{17} from locked-moment behavior at low temperature to superparamagnetic behavior at high temperature is more obvious in this case than in Fig. 15.

both of the aforementioned behaviors or the intermediate behavior. The sizes of the observed magnetic moments per atom depend only slightly on cluster size. Most of these clusters exhibit predominantly locked-moment behavior between the temperatures 97 K and 247 K. Gd_{30} is the main exception, being superparamagnetic at all observed temperatures.

Deducing the internal magnetic moment per atom for a superparamagnetic particle requires the use of Eq. (3) to relate μ to the effective magnetic moment per atom, μ_{eff}. After all, μ_{eff} is what we determine when we measure μ_{expt}. A locked-moment cluster has no single value that can be used to determine its internal magnetic moment per atom. Instead, we must fit its entire deflection profile to the prediction of the locked-moment model.

The predictions of the locked-moment model will be discussed in the following section. For now, we will simply use those predictions to reduce what would otherwise be an enormous amount of data (hundreds of complete deflection profiles) to a realistic size. We have used the
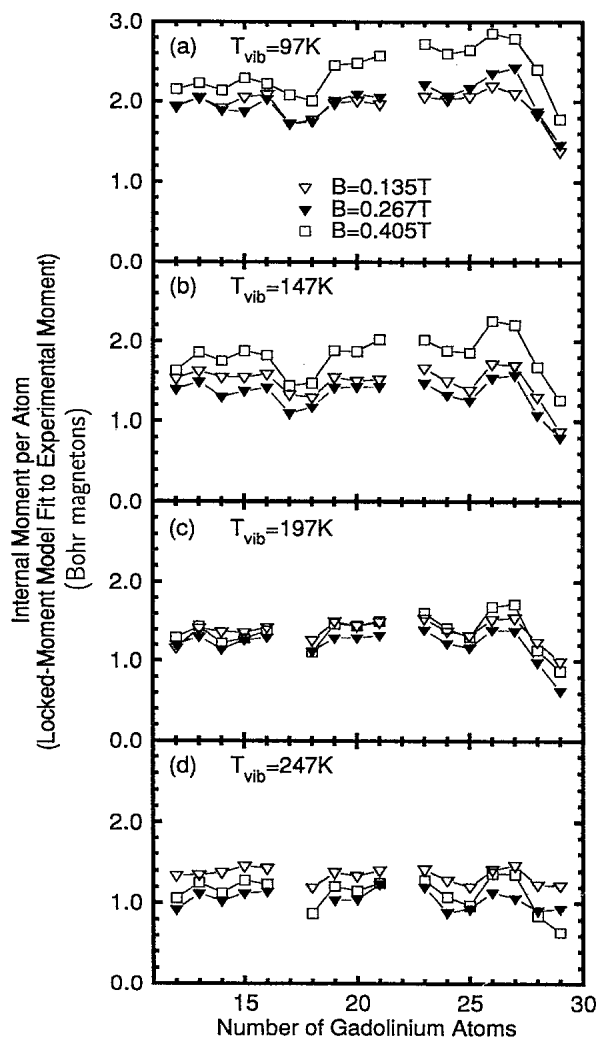

FIG. 17. Internal magnetic moment per atom versus cluster size, at four vibrational temperatures and three applied magnetic fields.

locked-moment model to obtain internal magnetic moments per atom of most of the clusters between Gd_{11} and Gd_{29} at four values of temperature and three values of applied magnetic field. The results are summarized in Fig. 17. We emphasize that any imperfections and oversimplifications in the locked-moment model will affect the values we report. Before we attempt to interpret this figure, we must discuss the locked-moment model in more detail.

B. Theory of locked-moment behavior

As we discussed in the Introduction, a cluster's magnetic moment may or may not be aligned with an easy axis of its lattice. The extent to which this alignment occurs depends on the cluster's vibrational temperature. At zero vibrational temperature, the alignment will be complete and the magnetic moment will be locked to an easy axis of the cluster. As the vibrational temperature increases, the alignment will become progressively less perfect and the cluster will eventually become superparamagnetic. We have already dealt with the superparamagnetic limit, where we assume that the cluster's magnetic moment is perfectly decoupled from its lattice. Now we will deal with the zero vibrational temperature limit where the cluster's magnetic moment is perfectly locked to its lattice. To make this study, we idealize the cluster as a spherical particle with its magnetic moment rigidly locked to its lattice.

The model system that we must understand is a spherical magnetic rotor in an external magnetic field. In our experiment, the clusters have an important, nonzero rotational temperature. No energy can flow from the rotational modes to the vibrational modes because of angular momentum conservation, so that we can model our clusters as having zero vibrational temperature but finite rotational temperature.

Our goal is to study the dynamics of a statistical ensemble of such rigid magnetic rotors and to determine the time-averaged projections of their magnetic moments on the magnetic-field gradient. Each cluster can be expected to have its own time-averaged magnetic-moment projection because its dynamics will depend sensitively on its initial conditions. This dependence on initial conditions produces an ensemble of clusters with different time-averaged magnetic moments and hence different deflections. One feature of this model is that it predicts broad deflection profiles like the ones that we observe experimentally.

We can treat the clusters classically, as they have very large angular momentum and spin quantum numbers. We consider a particular cluster size and model each cluster as a sphere with moment of inertia I, body-fixed magnetic moment μ, and angular momentum $I\omega$, that is precessing and nutating in an applied magnetic field $\mathbf{B}$. Each cluster has a magnetic potential energy $U_{mag} = \mu \cdot \mathbf{B}$ and a rotational kinetic energy $U_{rot} = I\omega^2/2$. If $U_{mag} \ll U_{rot}$, the angular momentum vector will simply precess around $\mathbf{B}$. If $U_{mag} \gg U_{rot}$, the cluster will oscillate like a pendulum, in and out of alignment with $\mathbf{B}$. If $U_{mag} \simeq U_{rot}$,

the cluster will undergo very complex precession and nutation that can only be followed by a computer.

The time-averaged projection of a cluster's magnetic moment on the field gradient, μ_{eff}, will depend strongly on that cluster's initial angular momentum vector, its initial magnetic-moment vector, the applied magnetic field, and how it enters that magnetic field. The applied magnetic field is ours to choose and the entry into the field is adiabatic. However, many initial angular momentum and magnetic-moment vectors are possible and must be considered. The magnitudes of these vectors are set by the rotational temperature of the supersonic cluster beam and the total magnetic moment of a cluster, but there are no restrictions on the initial angles.

To see that the entry into the magnet is adiabatic, consider a 23-atom cluster with $T_{rot} \approx 5$ K. This cluster will rotate many thousands of times during the approximately three-μs-long entry into the magnet. The applied field will change very little during each rotation, so the entry is adiabatic.

Since different initial conditions will yield different values for μ_{eff}, we must examine a statistical ensemble of initial configurations in order to determine the probability of observing a particular μ_{eff} and thus a particular deflection. At each applied field, a statistical ensemble is characterized by its rotational temperature T_{rot} and its magnetic moment μ. To produce a theoretical deflection profile for a particular choice of these two parameters, we numerically integrate the equations of motion for 10^7 different initial cluster configurations and fold in the spatial resolution. The different initial configurations are selected at random to produce isotropic distributions of the directions of μ and ω. A detailed description of the techniques used to obtain the predicted deflection profiles appears elsewhere.[21]

The model has only two parameters: rotational temperature, T_{rot}, and internal magnetic moment per atom, μ. Given these two parameters and the cluster size, the model predicts the deflection profile. We can vary the two parameters as we attempt to fit the predicted deflection profile to the experimental profile. Because most cluster sizes exhibit both locked-moment and superparamagnetic behaviors simultaneously, we add a third fitting parameter: the fraction of superparamagnetic clusters to superpose on the locked-moment component. These three parameters are varied to obtain the best fit to a given experimental deflection profile. This variation is accomplished numerically using the Levenberg-Marquardt method of nonlinear least-squares fitting.[22]

C. Interpretation of data

We have fit the predicted deflection profiles to the experimental profiles and obtained the internal magnetic moments per atom μ that are reported in Fig. 17. In all cases, the rotational temperatures T_{rot} used in the fits are approximately 5 ± 3 K. These rotational temperatures are relatively insensitive to the source temperature, but exhibit a moderate size dependence (they increase slightly with increasing size). The absence of a

discernible locked-moment component in Gd_{22} and Gd_{17} (above about 150 K) prevents us from including those two clusters in the data.

Our uncertainty in the values of μ obtained from the fitting process is approximately $\pm 0.15 \mu_B$/atom. This uncertainty is determined by the degree to which the predicted profiles fit the experimental profiles and the quality of the experimental data. The fits, some of which appear in Fig. 12, are not perfect and are particularly bad at high applied magnetic fields.

At each of four temperatures and three applied magnetic fields, we see that μ is relatively constant for all cluster sizes except Gd_{17}, Gd_{18}, Gd_{28}, and Gd_{29}. These four clusters show smaller μ than the other clusters. Gd_{17} is the cluster that undergoes the transition to superparamagnetic behavior between 100 K and 200 K, as discussed above. Its μ is omitted from Figs. 17(c) and 17(d) because there is no distinguishable locked-moment component. Gd_{29} is not particularly well fit by the locked-moment model at any temperature, nor is it well fit by superparamagnetism. It appears to be in some intermediate state, with its moment partially locked to its lattice, regardless of vibrational temperature.

The values of μ that we obtain by fitting the deflection profiles indicate a dependence of μ on both temperature and applied magnetic field. The decrease in μ with increasing temperature is large and reproducible. It is most likely due to a gradual failure of the locked-moment model with increasing vibrational temperature.

The locked-moment model assumes a magnetic moment that is rigidly attached to the lattice. As the vibrational temperature increases, that assumption becomes less valid. For Gd_{17}, the assumption fails completely somewhere between $T_{vib} = 100$ K and 200 K. The value of μ that we obtain for Gd_{17} at $T_{vib} = 147$ K is relatively small, suggesting that applying the locked-moment model to clusters that are approaching the transition to superparamagnetism will yield a value of μ that is smaller than it actually is. Because the transition temperature between locked-moment and superparamagnetic behaviors occurs somewhere around room temperature for all of these clusters,[5] the locked-moment model probably underestimates μ at the higher temperatures. This shortcoming of the locked-moment model does not rule out genuine changes in μ with temperature. The magnetic ordering of these clusters, whether ferromagnetic, antiferromagnetic, or both, is likely to be weak enough to be influenced significantly by the clusters' vibrational temperatures.

Figure 17 also shows some dependence of μ on applied magnetic field. At the higher vibrational temperatures, the small changes of μ with field are within the experimental uncertainties. At $T_{vib} = 97$ K, the increase in μ at the highest applied field is real and reproducible. But more significant than the values for μ obtained from the fitting process is the decreased quality of the fit. In Fig. 12(c), we see that the data are drawn toward strong field relative to the predicted profile.

The shift of the experimental cluster intensity toward strong field may be due to experimental or physical effects. Experimentally, the cluster packet is large enough

that the clusters do not all experience precisely the same applied field or field gradient as they travel through the 250-mm-long gradient magnet. More importantly, the clusters begin to deflect as they travel through the magnet and those that move toward strong field will experience ever increasing fields as they deflect. The deflection of clusters during their passage through the magnet is a serious limitation on the size of the applied fields we can use. We can actually cause the clusters to strike the magnet's pole faces if we use fields that are too large. Our inability to apply a uniform, constant field and field gradient to all clusters for the duration of their travels through the gradient magnet certainly contributes to the imperfect fit.

A more physical issue that may also contribute to the imperfect fit is the finite coercivity of the clusters. The locked-moment model assumes moments that are rigidly attached to the cluster lattice, regardless of applied field. Even if the cluster vibrational temperature is zero, that idealization becomes unrealistic at very large applied fields. In a real cluster, the magnetic moment is held in place by a crystal field. If the applied magnetic field is comparable to the crystal field, then it will compete with the crystal field for the attention of the magnetic moment. As the cluster rotates, precesses, and nutates about the applied field, its magnetic moment will tend to be drawn toward alignment with the applied field. The magnetic moment will not follow the easy magnetization axis of the cluster perfectly. This pulling of the cluster magnetic moment away from the easy axis will tend to shift the deflection profile toward strong field. In effect, the magnetic-moment vector begins to have some component of field-induced superparamagnetic behavior superposed on its locked-moment behavior.

Thus, the apparent increase in μ at high magnetic fields may be simply an indication that the locked-moment model is failing at these fields. There is a limit to the coercivity of the clusters. It is actually remarkable that the clusters are able to keep their magnetization vectors nearly aligned with their lattices, even in the presence of external fields approaching $\frac{1}{2}$ T.

V. CONCLUSION

We have found that cobalt clusters ($N = 65$–215) are superparamagnetic at vibrational temperatures between 85 K and 300 K. They have an internal magnetic moment per atom, μ, of $2.24 \pm 0.14\mu_B$/atom. This μ is substantially larger than the bulk value of $1.71\mu_B$/atom.

At vibrational temperatures between 97 K and 247 K, gadolinium clusters exhibit both superparamagnetic and locked-moment behavior. Both behaviors are present simultaneously among clusters of most sizes at the lower vibrational temperatures. The fractions of clusters exhibiting each behavior are dramatically cluster size dependent. As the vibrational temperatures increase, some of the locked-moment clusters evolve into superparamagnets. At temperatures somewhat below the transition temperature, the clusters exhibit magnetic behaviors that are neither purely superparamagnetic nor locked-moment.

At least one of the clusters that is predominantly superparamagnetic at all vibrational temperatures studied (Gd_{22}) has an internal magnetic moment per atom that increases with increasing temperature. This temperature dependence is consistent with a model in which the magnetic ordering of the cluster is antiferromagnetic. Antiferromagnetic ordering would also explain why the internal magnetic moments per atom that we observe in gadolinium clusters are much less than the bulk value.

We also find temperature and field dependences in the calculated internal magnetic moments of locked-moment gadolinium clusters. These dependences may be due, at least in part, to oversimplifications in the locked-moment model. At finite vibrational temperatures and in strong applied fields, clusters' magnetic moments will not remain perfectly aligned with their easy magnetic axes.

* Present address: Institut de Physique Expérimental, Ecole Polytechnique Fédérale de Lausanne, PHB-Ecublens, 1015 Lausanne, Switzerland.

[1] D. M. Cox, D. J. Trevor, R. L. Whetten, E. A. Rohlfing, and A. Kaldor, Phys. Rev. B **32**, 7290 (1985).

[2] W. A. de Heer, P. Milani, and A. Chatelain, Phys. Rev. Lett. **65**, 488 (1990).

[3] J. P. Bucher, D. C. Douglass, and L. A. Bloomfield, Phys. Rev. Lett. **66**, 3052 (1991).

[4] S. N. Khanna and S. Linderoth, Phys. Rev. Lett. **67**, 742 (1991).

[5] D. C. Douglass, J. P. Bucher, and L. A. Bloomfield, Phys. Rev. Lett. **68**, 1774 (1992).

[6] P. A. Hackett (unpublished).

[7] M. E. Geusic, M. D. Morse, S. C. O'Brien, and R. E. Smalley, Rev. Sci. Instrum. **56**, 2123 (1985).

[8] J. P. Bucher, D. C. Douglass, and L. A. Bloomfield, Rev. Sci. Instrum. **63**, 5667 (1992).

[9] D. McColm, Rev. Sci. Instrum. **37**, 115 (1966).

[10] K. D. Kolenbrander and M. L. Mandich, J. Chem. Phys. **92**, 4759 (1990).

[11] P. Milani and W. A. de Heer, Phys. Rev. B **44**, 8346 (1991).

[12] A. J. Cox and L. A. Bloomfield (unpublished).

[13] S. J. Riley, Phase Trans. **24**, 271 (1990).

[14] I. S. Jacobs and C. P. Bean, in *Magnetism*, edited by G. T. Rado and H. Suhl (Academic, New York, 1963).

[15] J. G. Louderback and L. A. Bloomfield (unpublished).

[16] T. Kasuya, in *Magnetism*, edited by G. T. Rado and H. Suhl (Academic, New York, 1966), Vol. IIB.

[17] A. J. Freeman, in *Magnetic Properties of Rare Earth Metals*, edited by R. J. Elliot (Plenum, London, 1972), pp. 245–333.

[18] J. P. Bucher and L. A. Bloomfield, Phys. Rev. B **45**, 2537 (1992).

[19] B. V. Reddy and S. N. Khanna, Phys. Rev. B **45**, 10 103 (1992).

[20] A. M. Spencer, D. C. Douglass, and L. A. Bloomfield (unpublished).

[21] L. A. Bloomfield (unpublished).

[22] W. H. Press, B. P. Flannery, S. A. Teukolsky, and W. T. Vetterling, *Numerical Recipes: The Art of Scientific Computing* (Cambridge University Press, Cambridge, 1986).